JCTC Journal of Chemical Theory and Computation

pubs.acs.org/JCTC Article

Atomistic Mechanisms of Binary Alloy Surface Segregation from Nanoseconds to Seconds Using Accelerated Dynamics

Richard B. Garza, Jiyoung Lee, Mai H. Nguyen, Andrew Garmon, Danny Perez, Meng Li, Judith C. Yang, Graeme Henkelman, and Wissam A. Saidi*

Cite This: J. Chem. Theory Comput. 2022, 18, 4447−4455 Read Online

ACCESS | Metrics & More | Article Recommendations | Supporting Information

ABSTRACT: Although the equilibrium composition of many alloy surfaces is well understood, the rate of transient surface segregation during annealing is not known, despite its crucial effect on alloy corrosion and catalytic reactions occurring on overlapping timescales. In this work, CuNi bimetallic alloys representing (100) surface facets are annealed in vacuum using atomistic simulations to observe the effect of vacancy diffusion on surface separation. We employ multi-timescale methods to sample the early transient, intermediate, and equilibrium states of slab surfaces during the separation process, including standard MD as well as three methods to perform atomistic, long-time dynamics: parallel trajectory splicing (ParSplice), adaptive kinetic Monte Carlo (AKMC), and kinetic Monte Carlo (KMC). From nanosecond (ns) to second timescales, our multiscale computational methodology can observe rare stochastic events not typically seen with standard MD, closing the gap between computational and experimental timescales for surface segregation. Rapid diffusion of a vacancy to the slab is resolved by all four methods in tens of nanoseconds. Stochastic re-entry of vacancies into the subsurface, however, is only seen on the microsecond timescale in the two KMC methods. Kinetic vacancy trapping on the surface and its effect on the segregation rate are discussed. The equilibrium composition profile of CuNi after segregation during annealing is estimated to occur on a timescale of seconds as determined by KMC, a result directly comparable to nanoscale experiments.

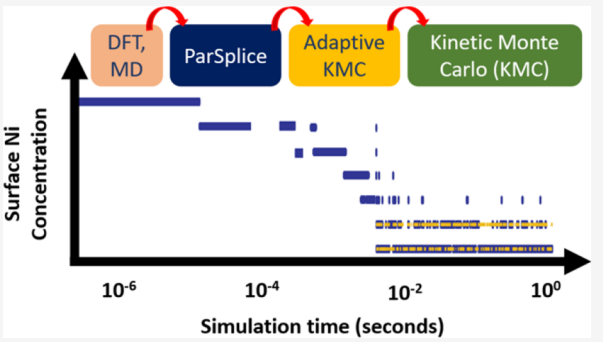

1. INTRODUCTION

Alloy surfaces are typically enriched with one of their constituent elements, particularly in the top layers, because of differences in the surface energies of pure metals. This surface segregation process leads to metallic demixing, which is of relevance to many different fields of research such as catalysis and metallurgy, considering that in situ transformations can affect the chemical activity or structural integrity gained from homogeneously alloying pure metals together. Alloy surface segregation and ordering has been measured experimentally both in vacuum and gas environments, with differences in the equilibrium alloy composition induced near the exposed top layers for many bimetallic alloys.[1−6] Consequently, studies of alloy surface transformations are influenced by prior phase separation in vacuum during pretreatment. A decoupling of the experimental environment from the pretreatment environment is required to understand the transient effect on nonequilibrium surface composition because nanoscale elemental mapping is not feasible on relatively short microsecond (μs) timescales even using electron and X-ray diffraction.

Molecular dynamics (MD) simulations can generally resolve atomic transitions on the picosecond (ps) to nanosecond (ns) timescales. While these short timescale dynamics can be easily investigated using energetic models based on either classical force fields or first-principles methods, longer timescales that are often more relevant experimentally are challenging to realize with conventional resources and techniques.[7−9] As shown in the current work, alloy surface segregation occurs over millisecond (ms) timescales that are impractical to obtain using conventional MD simulations. This goal can be achieved with accelerated methods including adaptive kinetic Monte Carlo (AKMC) and temperature-accelerated dynamics (TAD).[10−12] These two methods were employed in a multiscale approach to study surface segregation in ceramics (rocksalt oxides) during oxidation.[13] Also, more recently, surface segregation and timescales in PdAu nanoparticles have been studied using AKMC.[14] However, alloy segregation and timescales related to the metallic dopant dynamics are not well

Received: March 29, 2022
Published: June 7, 2022

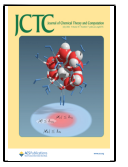

https://doi.org/10.1021/acs.jctc.2c00303
J. Chem. Theory Comput. 2022, 18, 4447−4455

understood in nanoscale thin films, as these require larger systems (>100 atoms) to accurately simulate the region between bulk and exposed surface. These larger, periodic systems can approximate the semi-infinite boundary for the dopant concentration present in thin films, which could differ from that of nanoparticle (NP)[15,16] systems at least for relatively small examples. In addition to varying finite-size effects between NPs of different sizes, NPs also exhibit strain responses from overall lower surface coordination near edges and vertices compared to pristine, periodic films without these edges. These strain effects result in core-shell structures for CuNi NPs that do not appear in thin films.[17,18] A recent KMC study investigated the dynamics in bulk NiFe solid solution, reporting that the vacancy migration barrier is highly influenced by the local composition, a behavior that the authors predict will influence the rate of microscale phase transformations.[19] Previously, only the dependence of activation energy on the overall alloy composition could be predicted or measured with any accuracy.[20] The failure of these global models for concentrated solid solutions is known, although they may be corrected by sampling transition energies in differing chemical environments.[21]

In this study, we model the nonequilibrium surface segregation process by employing multiscale simulation methods that probe the dynamics from picosecond to second timescales. We focus our investigations on cupronickel (CuNi), which exhibits surface segregation at elevated temperatures in vacuum, enriching with Cu near the surface and Ni in the bulk.[22,23] The CuNi alloy is of interest for different applications with extreme environmental conditions including marine settings because of its resistance to corrosion by seawater,[24,25] as well as a high-temperature catalyst for thermal CO_2-to-syngas-to-fuel conversion.[18,26−28]

To date, the transient dynamics of segregation in CuNi have not been investigated. Previous studies have employed Monte Carlo (MC) to show that the Ni solute concentration is significantly decreased in the top three surface monolayers for all slab orientations, approaching its value in the bulk at a depth of four or five atomic layers below the surface.[29−31] While MC simulations describe the systems in equilibrium, they do not give a timescale for the segregation process. In contrast, MD can provide a timescale for dynamics, but it has not been utilized before to study transient dynamics of the segregation process. Limited investigations of dislocation slip under applied stress (work hardening) or melting in CuNi[32,33] have been carried out using MD because these processes occur over ns timescales, yet the impact on larger-scale reordering on experimental timescales was not explored in those studies. Thus, the mechanism, as well as the timescale, for transformation from a randomly mixed to ordered alloy on the nano- and microscales remains unclear.

Accelerated methods can provide insight into longer timescales into atomistic mechanisms of surface segregation phenomena. Previously, AKMC investigations of the segregation kinetics of PdAu nanoparticles showed greater kinetic stability because of reduced strain in the mixed phase.[14] In the present work, we probe segregation dynamics in planar, (100) CuNi surfaces, employing conventional MD and three accelerated dynamics methods: parallel trajectory splicing (ParSplice), AKMC, and KMC with kinetic barriers derived from a cluster expansion. ParSplice affords accurate system evolution up to ∼10 μs, while AKMC and KMC simulate longer timescales up to ms and seconds, respectively.

ParSplice[11] extends MD simulation times by leveraging parallel computers to carry out parallelization in the time domain, in contrast to the usual spatial domain decomposition approaches.[34,35] Thus, with ParSplice, it is possible to simulate small systems over very long timescales, again in contrast to conventional parallelization approaches that are efficient at spatially decomposing large systems simulated on short timescales. This is accomplished by concurrently generating a large number of independent, short trajectory segments using a procedure that guarantees these segments can be assembled into a longer state-to-state trajectory that is statistically correct.[36] Many segments begin from the current state and evolve up to a user-specified time, typically reaching multiple unique endpoints before this time elapses. Periodic quenching is used to identify transitions between metastable states and distinguish segment terminations. Then, a unique hash and graph are provided for each segment to allow for rapid indexing from the database. It can be shown that ParSplice trajectories can become arbitrarily accurate by adjusting the estimate of the so-called correlation time of the dynamics, at the expense of a computational overhead.[37] When the dynamics follow from a sequence of rare events, ParSplice can provide a computational speedup that scales with the number of processors used; it is therefore especially powerful when deployed on massively parallel computers.

KMC-based methods do not have a fixed timestep; instead, they find the time elapsed for the first escape from one state to another, allowing for large periods of vibrational motion in the atomic system to be bypassed.[14,38] These escape times correspond to reaction rates, which are calculated adaptively or "on the fly" to construct an AKMC state model: nothing in the output event table is predefined or assumed from prior knowledge.[12,14,38] AKMC uses minimum-mode following searches or high-temperature MD to construct this event table: the transition state energies (activation barrier heights) are found using single-ended saddle point finding algorithms such as the dimer method.[39−41] To achieve further acceleration while maintaining as much of this accuracy as possible, in the present study, we use off-lattice dynamics from AKMC to fit a more approximate, lattice-based KMC model, which functionally depends on the Ni coordination via a cluster expansion.

Our multiscale approach produces a hierarchy of trajectory data for the segregation process over a broad range of timescales. To represent trajectory data on varying scales and fidelities, we track physical properties including the local defect chemical environment and its influence on the correlated rates of segregation and vacancy migration. Furthermore, we find that segregation in the top layer is a function of the rare reentry of a vacancy from the surface to the subsurface, which only occurs with a frequency of 10 μs because of a high kinetic barrier, greatly increasing the time required for the surface to be completely depleted of Ni. We also determine that the number of dopant atoms in the 1st and 2nd coordination shells around the point defect alters its migration energy, affecting the rate of composition change. The consistency of system evolution during segregation by thermal annealing across all the accelerated methods is examined on many timescales; this evidence supports each technique's further use in multiscale simulations in combination with the data processing methods used in this work.

https://doi.org/10.1021/acs.jctc.2c00303
J. Chem. Theory Comput. 2022, 18, 4447−4455

2. METHODOLOGY

2.1. Validation of the Embedded-Atom Method Potential. A reliable interatomic potential is required to obtain accurate MD of surface segregation and equilibrated structures. Here, we employed the embedded-atom model (EAM) potential of Fischer and collaborators, which is designed to model CuNi phase segregation across grain boundaries and is parameterized with surface energies, lattice constants, vacancy migration energies, and relevant quantities governing the rate of metallic phase separation.[42] We first verified the applicability of this potential to study CuNi surface segregation by comparison of calculated surface energies with those obtained from spin-polarized DFT calculations carried out using Vienna ab initio simulation package (VASP) with the Perdew−Burke−Enzerhof (PBE) exchange-correlation functional,[43−47] see SI Appendix A, Table A1. Furthermore, we verified that the segregation of Ni to the bulk—from the 1st to the 2nd or 3rd layer—is always favorable, that is, $\Delta E_{\mathrm{Ni,surf}\rightarrow\mathrm{interior}} \approx -0.4$ to -0.3 eV from DFT and EAM, also in agreement with previous ab initio calculations.[48] Furthermore, we found good agreement with the previously reported anisotropic, thermodynamic tendency for Ni to segregate to exposed <100> and <110> facets in favor of <111> surfaces.[23,30]

2.2. Slab Models and the Initial State for Annealing. We employed slab models of the (100) surface termination that are composed of 216 and 384 atoms by randomly substituting Cu with Ni. These slabs were 12 monolayers in thickness with 3 × 3 and 4 × 4 surface periodicity; nearly doubling the vacancy concentration (1:216 vs 1:384 atoms) did not affect our observed mechanisms or energetics. Thus, systems of smaller surface periodicity (3 × 3, 216 atoms) were simulated to realize the longest timescales for higher fidelity time-averaging and activation energy histograms. MC simulations across the composition range of 2.7−16 at% Ni and a temperature range of 300−700 K showed no detectable variation in the amount of Ni segregated. For this reason, we chose to exclusively simulate systems with 16 at% Ni at 500 K with the accelerated MD methods.

The equilibrium composition profile of the CuNi (100) surface alloy is determined using MC. The method attempts 10^6 MC swaps of Cu and Ni atoms with subsequent minimization and an acceptance probability as determined via the Metropolis algorithm.[49] MC composition profiles are found to be consistent with similar reported profiles[22,29−32,50] across a range of compositions and temperatures, see SI Appendix B. Such agreement with previous computational and experimental results is a further validation of the reasonable accuracy of the EAM potential.

2.3. Multiscale Simulation Hierarchy. The methods employed in our multiscale hierarchy are described as follows, in the order of accessible timescale: MD in the NVT ensemble was generated using a Langevin thermostat, as implemented in the large-scale atomic/molecular massively parallel simulator (LAMMPS) code.[51] Because the low temperature (500 K) used in the work negligibly alters the alloy lattice spacing, the structures do not require NPT equilibration of the system and slab volumes. Furthermore, ParSplice, AKMC, and KMC do not yet have simulations in NPT ensemble implemented, although this may change in the future. Our simulation approach fixes the slab volume during the equilibration and production phases by maintaining a constant surface area for both sides of the slab.

Many instances of LAMMPS were then orchestrated by the EXAALT/ParSplice code [http://gitlab.com/exaalt] to carry out long-time ParSplice simulations. Direct MD realized nanoseconds of simulated time using the velocity Verlet algorithm and modest resources (4 processors). ParSplice accelerated these dynamics up to μs timescales using 224 processors. Both standard MD and ParSplice were carried out in the same way: after initializing particle velocities according to a Boltzmann distribution representing the target temperature, the systems were equilibrated with a 2 fs timestep and a 1 ps temperature relaxation time for 200 ps. Multiple random number seeds are used by ParSplice to initialize system velocity many times during replica dynamics, allowing exploration of the local state space to identify new segments.[35] The first segment identified escaping to a new state is appended to the end of the parallel trajectory. After the equilibration phase of MD, a further 400 ns were simulated to constitute the production phase, while ParSplice was employed to accelerate this simulation time up to 35 μs. Minimization was done with the conjugate gradient algorithm using convergence criteria of 10^{-8} eV and 10^{-6} eV/Å for the energy and forces,[52] respectively. These quenching parameters are also used by ParSplice to identify state transitions and properly terminate each parallel MD replica.

In contrast to ParSplice and MD, the AKMC and KMC models use a nonconstant timestep, which varies to match the timescale of the first escape time from a given state. Over longer timescales, up to many seconds, KMC-based acceleration approaches the segregation found with MC.[12,38] KMC methods simulate the time evolution of the system, requiring a predetermined event table in which the kinetic rate of each event is approximated through the Arrhenius relation to the precalculated activation energy. At each step, a random event i is selected from the table in the order from 1 to i with the condition

$$\sum_{1}^{i-1} r_{i-1} < p_1 \sum_{1}^{N} r_N \leq \sum_{1}^{i} r_i$$

where $\sum_1^i r_i$ is the sum of the rate from event 1 to event i, $\sum_1^{i-1} r_{i-1}$ is the sum of the rate from event 1 to event $i-1$, p_1 is a random number between 0 and 1, and $\sum_1^N r_N$ is the total rate of the event table. Time is then incremented by

$$\frac{-\ln(p_2)}{\sum_1^N r_N}$$

where a random number p_2 is drawn between 0 and 1. AKMC allows the system to find all potential events without a predetermined event table.[45] In order to search for events, AKMC uses high-temperature MD and the climbing-image nudged elastic band (CI-NEB) approach to calculate the saddles for the new states using the EON software.[53]

To reach even longer timescales with KMC, an energy estimation based on the local environment of the vacancy was generated by a cluster expansion. The energy was predicted to be dependent on the concentration of Ni and Cu located in the first nearest neighbor shell of the vacancy. In the FCC CuNi alloy, there are 8 nearest neighbors for the vacancy on the surface and 12 nearest neighbors for the vacancy in the subsurface. Sequentially, the energy-fitting model was used to determine the barrier and rate of the events in the event table

https://doi.org/10.1021/acs.jctc.2c00303
J. Chem. Theory Comput. 2022, 18, 4447−4455

based upon the trajectory data from our AKMC simulations. More information about the cluster expansion method is provided in the SI, Appendix C. Furthermore, we found satisfactory agreement between AKMC and KMC by carrying out the dynamics up to 300 μs, further validating the KMC model (see SI, Appendix D).

Finally, the concept of an equilibrium rate was introduced to further accelerate the timescale accessible by KMC. In this approximation, no rate was allowed to be larger than the specified equilibrium rate with the assumption that all states connected by rates faster than the equilibrium rate should already be in equilibrium. In the case of CuNi segregation, the planar diffusion of a vacancy on the exposed surface is rapid, equilibrating on much shorter timescales than for defect re-entry to the subsurface to occur even once. Ultimately, the effect of an artificial equilibrium rate in KMC simulations is that these key transitions can be sampled more effectively instead of the many horizontal transitions that do not alter the composition with respect to the surface depth.

In both AKMC and KMC simulations, the temperature was set to 500 K, and the prefactor for the rates was fixed at 5×10^{12} s^{-1}. The optimizer used in AKMC was L-BFGS, with a convergence criterion of 0.01 eV/Å.[53] System evolution from AKMC reached ms timescales running for a week on 24 cores. The following KMC timings are the average of five separate runs in both cases: KMC realized seconds of simulation time running on a single processor for 2 h with the added equilibration rate. KMC without the equilibrium rate was only simulated up to 10 ms because only 1 min of wall clock time was necessary before the surface vacancy trapping described above halted Ni segregation in the system.

3. RESULTS AND DISCUSSION

The equilibrium composition profiles obtained with MC (Figure 1) exhibit Ni migration out of the top three surface layers, while the concentration of the fourth and fifth layers approach the bulk value. This trend did not quantifiably vary with changes in system temperature or Ni concentration. The near-surface Ni concentration observed with the EAM potential agrees with the profiles derived from previous MC simulations[22,29−32] as well as experiments.[1−3,23]

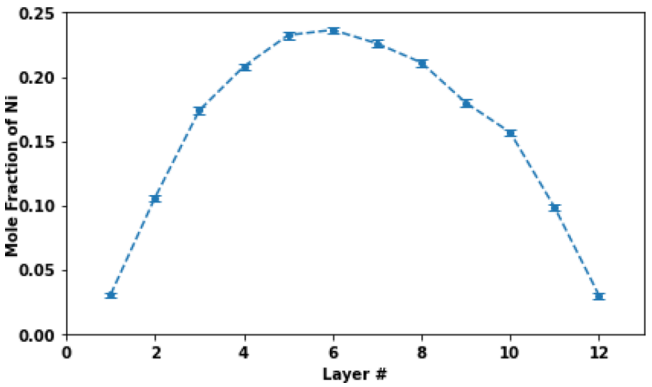

Figure 1. Ni composition profiles of Cu−16at%Ni (100) surface as a function of the layer depth after MC annealing at 500 K. The slab has 12 layers with layers 1 and 12 exposed to the vacuum. Composition is normalized by the number of atoms in a pristine FCC <100> layer (18), resulting in a mismatch between the bulk composition of layer 6 (~22 at% Ni) and the overall composition (16 at% Ni).

Next, we probed the segregation dynamics using MD, ParSplice, AKMC, and KMC, starting from the same initial configuration of the random alloy. Lattice vacancies are the primary defect responsible for alloy segregation: the only other mechanism, self-interstitial migration of metal atoms to octahedral or tetrahedral sites, is destabilized by greater formation and migration energies than those for the point defect (vacancy).[54] Hence, our simulations included a single vacancy to facilitate surface segregation.

Figure 2 shows the composition over time within the top layer of our Cu−16at%Ni (100) slab model for a single simulation of each type within our methodology. The concentration of Ni atoms in the top surface layer decreases over time as it transitions from a uniform distribution to that of equilibrium, as shown by the MC simulations in Figure 1. The accessible simulation time increases sequentially for each method (MD, ParSplice, AKMC and KMC). In MD (Figure 2a), the vacancy diffuses to the surface at 0.3 μs, displacing a Ni atom to the subsurface; up to the total time of 0.4 μs, the vacancy remains trapped on the surface so that the Ni concentration does not change. With over 30 different MD simulations, we observed that the time for vacancy percolation to the surface was consistently less than 1 μs, resulting in similar degrees of segregation, as shown in Figure 2a.

ParSplice (Figure 2b) shows similar dynamics as in standard MD, with vacancy migration to the surface in a fraction of a μs. Throughout the simulation, the ParSplice trajectory visited 8,278 topologically unique states while making 37,458 transitions, the vast majority of which occurred after the vacancy had reached the surface. The parallel acceleration of ParSplice increased the timescale from the standard MD simulation by a factor of ~100 up to 35 μs, but even at this longer timescale, the vacancy remained trapped on the surface, and no additional Ni segregation was observed. As expected, ParSplice is consistent with MD on timescales where they overlap (0.4 μs) not only in terms of bulk vacancy diffusion but also the timescale at which the vacancy diffuses to the surface. We have repeated the ParSplice simulations dozens of times with different random seeds observing early vacancy diffusion to the surface (before 1 μs) in nearly all trials, just as with MD.

With AKMC, we increased the simulation timescale by another order of magnitude (Figure 2c): a total of 144,597 transitions evolved the system through 32,369 unique states (a similar ratio of transitions to new states found as in ParSplice). It should be noted that our AKMC approach uses coarse-graining following the MC with the absorbing Markov chains (MCACM) method, allowing many more transitions to be considered via an analytic solution to the rate equations.[55] From the AKMC dynamics, we can observe events in which the vacancy moves from the surface to the subsurface at a timescale of roughly 50 μs. Over the simulation time of 300 μs, five such events were observed, resulting in two Ni atoms and three Cu atoms migrating from the surface to the subsurface.

With our KMC model (Figure 2d), we executed 4.7 million transitions generating 10 ms of simulated time. Over these timescales, the system appears to approach equilibrium, with fluctuations in the surface concentration between 0 and 5% Ni. However, what is not obvious from these plots is that the vacancy spends all of its time in the first and second layer, so that Ni segregation only occurs between the surface and subsurface layers. This behavior originates from a disparity in barrier heights that embodies the "low-barrier problem," more aptly referred to as the "heterogeneous barrier" problem.

https://doi.org/10.1021/acs.jctc.2c00303
J. Chem. Theory Comput. 2022, 18, 4447−4455

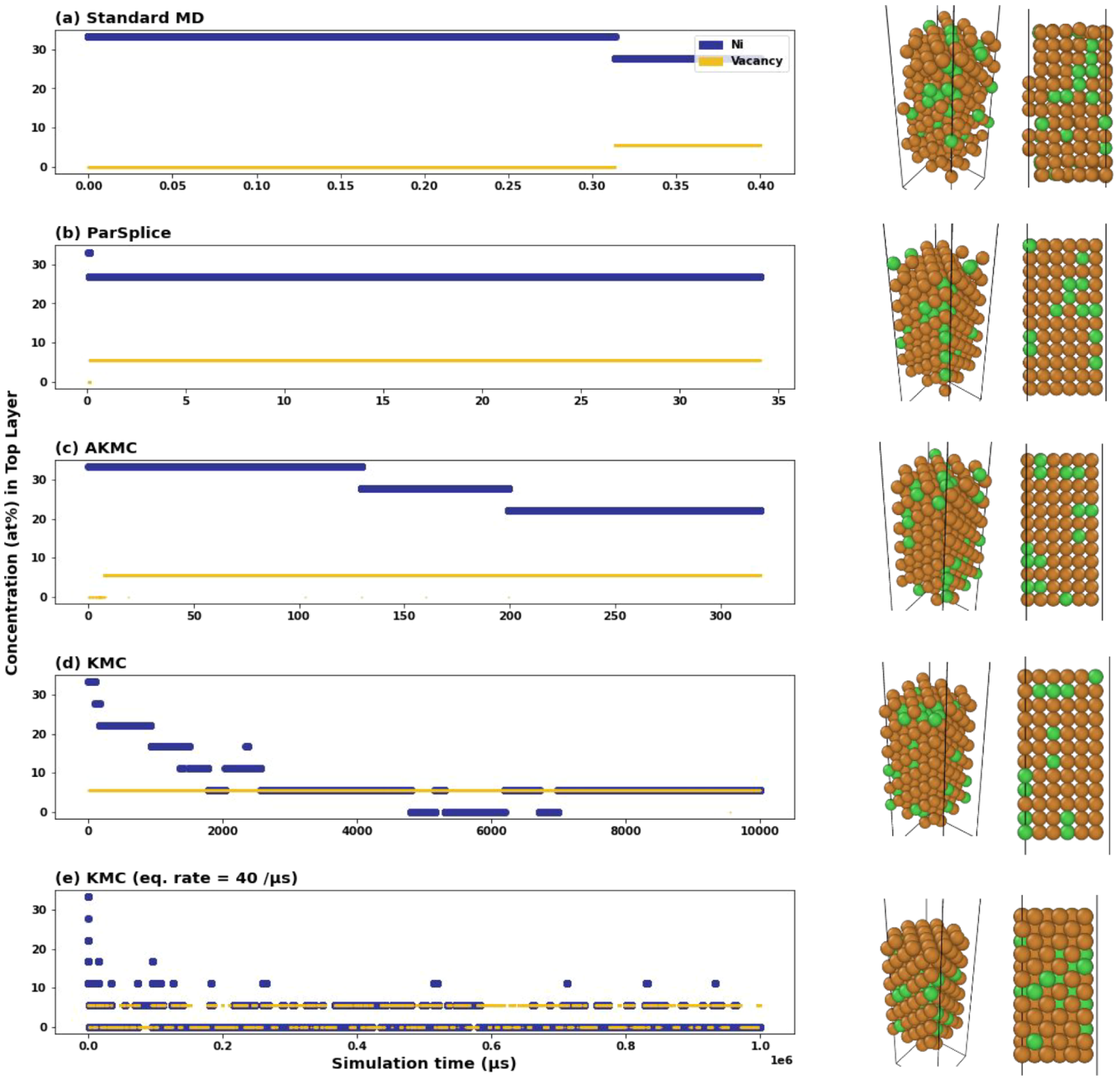

Figure 2. (left) Ni content in the top layer of Cu−16at%Ni(100) with a vacancy for (a) standard MD, (b) ParSplice, (c) AKMC, (d) KMC, and (e) KMC with applied equilibrium rate. Composition is normalized as in Figure 1. (Right) Orthographic and side views of the final slab model from each simulation are provided for reach simulation.

Dynamics with a mix of low and high activation barriers are inherently more difficult to accelerate because groups of states interconnected by low barriers will always dominate the trajectory during naive state space exploration.[8,11] The barrier for vacancy surface diffusion is 0.4−0.5 eV, whereas the barrier for the vacancy to go subsurface is 0.8−0.9 eV. Thus, we are simulating on the order of a million KMC steps with the vacancy mostly diffusing on the surface for one subsurface diffusion event, offering a low chance for segregation to occur. Even factoring in the small cost of each KMC step, this makes it impossible to simulate an equilibrium distribution of Ni in the top three layers.

To further accelerate the dynamics and mitigate the "heterogeneous barrier" problem, in our final simulation (Figure 2e), we perform KMC with the equilibrium rate approximation described in the Methods section, realizing 160 million transitions to reach a simulated time of 1 s. Here, the idea is that the vacancy will quickly reach local equilibrium diffusing in the top layer, and no new states of interest are explored until subsurface diffusion occurs. Because vacancy surface diffusion occurs on a timescale of ns, and diffusion of the vacancy to the subsurface occurs on a timescale of μs, we chose an equilibrium rate of 40/μs to slow the surface diffusion and accelerate the diffusion of the vacancy to the subsurface and below. Figure 2e shows that on a timescale of seconds, the surface Ni concentration fluctuates around equilibrium after 0.4 s until the end of our simulation lasting 1 s.

https://doi.org/10.1021/acs.jctc.2c00303
J. Chem. Theory Comput. 2022, 18, 4447−4455

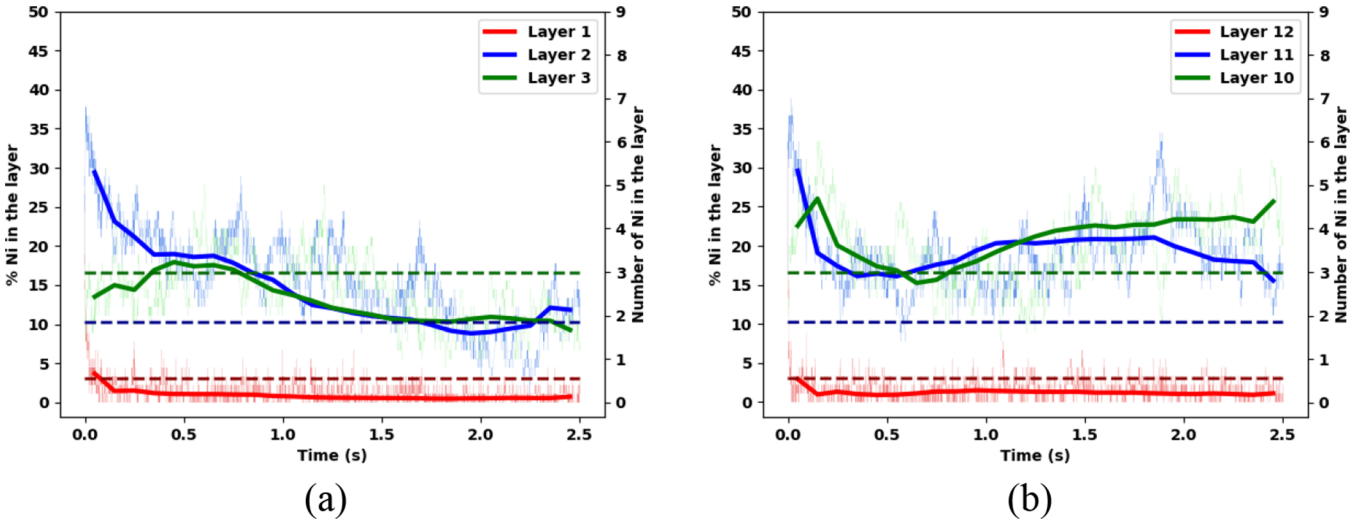

Figure 3. Ni composition averaged over five KMC simulations for the (a) bottom three layers and (b) top three layers over 2.5 s with an equilibrium rate of 40/μs. The bold line represents the 0.5-second-average calculated from the lighter single-frame datapoints, and the dashed line corresponds to the average concentration of Ni by MC calculation with the EAM potential at each layer when the system moves toward equilibrium. Composition is normalized as in Figure 1.

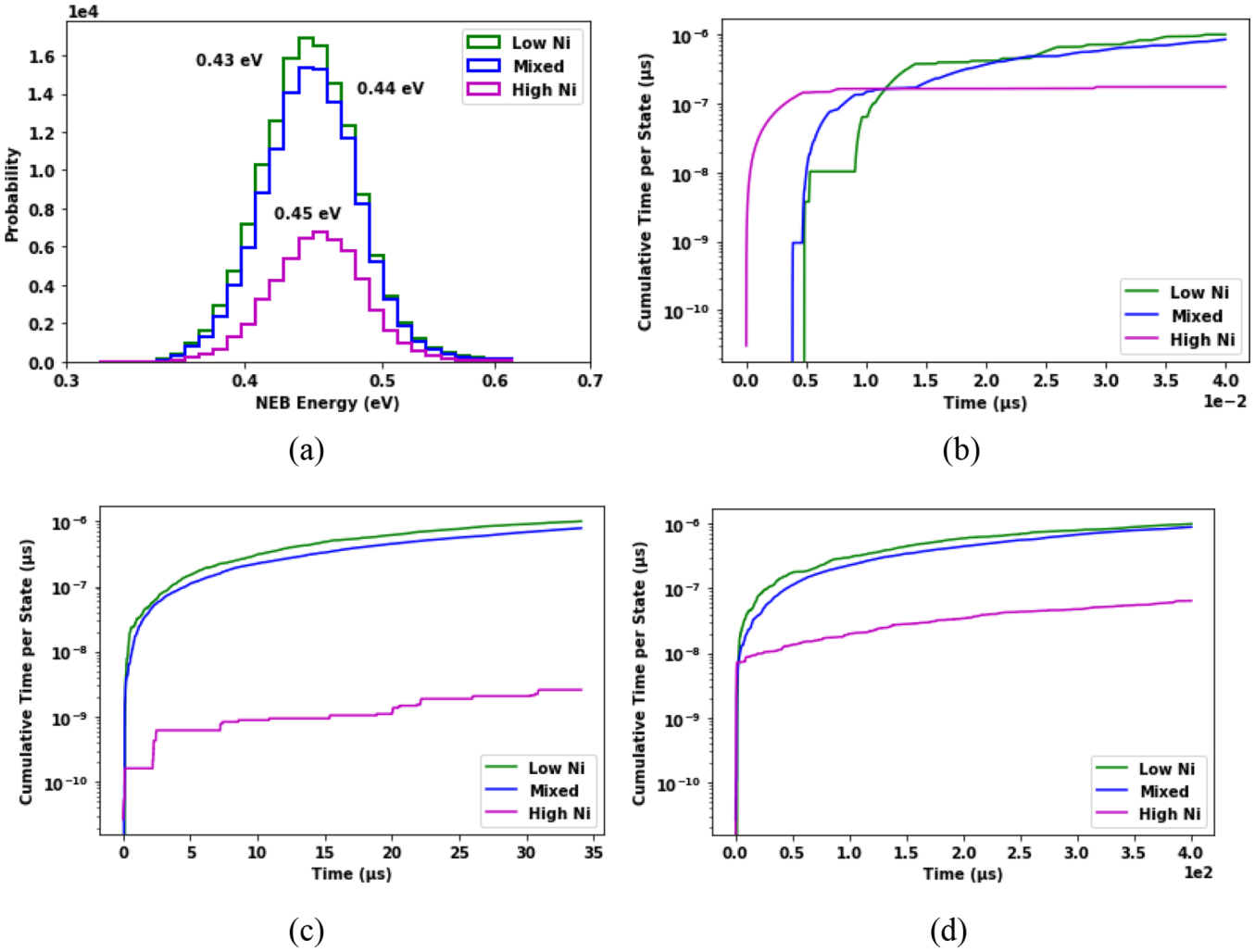

Figure 4. (a) Histogram of vacancy migration energy barriers obtained from a 319 μs AKMC simulation. (b−d) Total residence time for the vacancy in different chemical environments for (b) MD, (c) ParSplice, and (d) AKMC. Cumulative times are normalized by the prevalence of each composition type in the system rendering them unphysical.

https://doi.org/10.1021/acs.jctc.2c00303
J. Chem. Theory Comput. 2022, 18, 4447−4455

In order to more accurately estimate the timescale required to obtain the equilibrium profile, we performed five individual KMC simulations with the same equilibrium rate ($40/\mu s$), extending the total time to 2.5 s corresponding to about 400 million transitions. Although we utilize the per-layer final compositions previously shown in Figure 1 from MC annealing as a predictor for the local equilibrium composition, the moving average for local concentration from KMC may continue to fluctuate after this target composition is first realized. Figure 3 shows the moving average of Ni composition obtained from these KMC simulations in the bottom three layers (referred to as layer 1, 2, and 3) and the top three layers (referred to as layer 12, 11, and 10) in bold lines compared with the corresponding, nonmoving average equilibrium layer compositions obtained by MC (data from Figure 1) in dashed lines. From Figure 3a, we can see that layer 1 reached the MC value in less than 0.1 second and even approached zero Ni concentration at ∼1.5 s, although this does not occur in MC annealing on average, during which a single Ni atom remained on the surface for most of the equilibrium samples (Figure 1). Layer 2 exhibits more dramatic changes. The local composition started from 30% Ni, dropped to the MC composition of 10 at % ∼1.75 s, and remained near the estimated value from MC profiles until the end of the simulation. While the MC simulation left 16% Ni in layer 3, our KMC model shows more Ni segregations, leaving 10% Ni in the layer. This might explain the higher Ni composition profiles of the top two sublayers (layer 11 and 10) in Figure 3b. While layer 12 shows similar behavior as layer 1, layer 11 did not reach the MC profile until 2.5 s when its composition started to move toward MC composition, and layer 10 first reaches the MC profile at ∼0.6 s before the composition increased again. The overall profile, nonetheless, clearly shows an increase in the number of Ni atoms in bulk layers, indicating thermodynamic tendency for this dopant to remain in the bulk rather than on the surface. The state space exploration from KMC is inherently much greater than that of MC, which is not a dynamical method and can only follow an unphysical trajectory toward the lowest system energy.

Apart from surface effects, the local chemical environment around a vacancy is expected to determine the system energetics and the rate of Ni composition change. To investigate this, we tracked the number of Ni atoms within a 5 Å radius of the vacancy. The number of Ni atoms in the local environment ranges from 0 to 12, with three distinct "bins" of equal width formed for low, mixed, and high Ni content environments. The spectrum of barriers calculated during AKMC for all vacancy migration events within this trajectory is presented as a histogram in Figure 4a, which shows the lowest transition state energies for vacancy migration in Ni-rich regions of the alloy. Additionally, because the system has lower Ni content than Cu, the probablities are smaller for transitions into/within Ni-rich regions than for those with mixed and Cu-rich compositions. Vacancy migration energies are shifted closer to 0.4 eV in the Ni-rich regions than for migration in Cu-rich regions according to Figure 4a. We can deduce that vacancy migration is favored in the Ni-rich regions, contributing to the lower dwell time near Ni as the vacancy more rapidly diffuses toward and away from this dopant. Vacancies must slowly explore the Cu-rich regions of the host lattice before returning to possibly segregate the Ni atoms away from the surface. The order of the normalized, integrated peak areas in Figure 4a also supports this conclusion.

The overall time spent in low Ni, mixed, and high Ni content environments is also shown with respect to time in Figure 4b−d using a cumulative measure of residence time for MD, ParSplice, and AKMC and rescaling this measure by the prevalence of each environment in the system. The number of Ni atoms in the vicinity of the vacancy modulates these timescales substantially but in a similar fashion for all methods. Furthermore, the logarithmic trendlines and their orders of magnitude agree across overlapping timescales for MD/ParSplice (ns) and ParSplice/AKMC (μs): this supports the hierarchy of methods utilized herein as a theoretical foundation to connect correlated observations evolving across many timescales for the same process. The cumulative dwell time and thermodynamic trends match for all of the simulation methods in the order of integrated peak areas (Figure 4a) and residence times (Figure 4b−d): $t^{\text{total}}_{\text{Cu}-\text{rich}} > t^{\text{total}}_{\text{mixed}} > t^{\text{total}}_{\text{Ni}-\text{rich}}$. Although this agreement does not hold at very early (ps) simulation times with low cumulative sums, particularly for MD which is noisier compared to accelerated methods, the trend becomes evident in the ergodic limit. The residence times of vacancy chemical environment presented in Figure 4b−d confirm that the local composition is an effective determinant of where a vacancy spends most of its time during annealing and segregation. Specifically, the position of Ni in the lattice is a minor determinant of the dynamics because the dopant slightly biases the vacancy's random walk by ∼0.1 eV. This effect has also been documented in Ni−Fe surfaces annealed at 1100 K using KMC, where the local composition and the identity of the atoms exchanging during segregation (solute vs solvent) significantly influenced the vacancy migration energy and the measured tracer diffusion coefficient.[19]

4. CONCLUSIONS

In summary, we have applied three accelerated dynamics methods to examine the rate of segregation in CuNi alloy from nanosecond to second timescales, reaching 2 s of simulation time and the equilibrium composition with KMC. This composition profile shows no Ni on the top surface monolayer, with less than 15at% Ni in the second layer compared to 22at% Ni in the bulk on a per-layer basis, in agreement with MC predictions. Although most of our accelerated methods were used to simulate up to the μs timescale, only modified KMC dynamics could reach the equilibrium profile obtained from MC and previous experimental observations. Our model estimates that the timescale for segregation in the top layer to reach equilibrium is on the order of 0.1 ms, while equilibrium segregation does not penetrate to the 3rd layer until timescales on the order of 100 ms. The equilibrium timescales for surface segregation of any FCC bimetal can be determined with a combination of AKMC and KMC. However, KMC-based methods require assumptions regarding the transition state theory, and they do not resolve fast atomic exchange processes as well as ParSplice and MD. Our study shows that a model for the relationship between solvent distribution, activation energy, and large-scale phenomena like segregation may be developed from further simulations of bimetallics on experimental timescales. Our methodology is general and can be applied in the future using other interatomic potentials, including those derived from machine learning.[56−60]

https://doi.org/10.1021/acs.jctc.2c00303
J. Chem. Theory Comput. 2022, 18, 4447−4455

■ ASSOCIATED CONTENT

Supporting Information

The Supporting Information is available free of charge at https://pubs.acs.org/doi/10.1021/acs.jctc.2c00303.

Description of DFT validation of the EAM interatomic potential, composition measurements from MC data, cluster expansion model for kinetic Monte Carlo (KMC) simulation, comparison of AKMC and KMC results (PDF)

■ AUTHOR INFORMATION

Corresponding Author

Wissam A. Saidi − *Department of Mechanical Engineering and Materials Science, University of Pittsburgh, Pittsburgh, Pennsylvania 15260, United States;* orcid.org/0000-0001-6714-4832; Email: alsaidi@pitt.edu

Authors

Richard B. Garza − *Department of Mechanical Engineering and Materials Science and Department of Chemical and Petroleum Engineering, University of Pittsburgh, Pittsburgh, Pennsylvania 15260, United States*

Jiyoung Lee − *Department of Chemistry and Oden Institute for Computational Engineering & Sciences, University of Texas at Austin, Austin, Texas 78712, United States*

Mai H. Nguyen − *Department of Chemistry, University of Texas at Austin, Austin, Texas 78712, United States*

Andrew Garmon − *Theoretical Division T-1, Los Alamos National Laboratory, Los Alamos, New Mexico 87545, United States; Department of Physics & Astronomy, Clemson University, Clemson, South Carolina 29631, United States*

Danny Perez − *Theoretical Division T-1, Los Alamos National Laboratory, Los Alamos, New Mexico 87545, United States;* orcid.org/0000-0003-3028-5249

Meng Li − *Department of Chemical and Petroleum Engineering, University of Pittsburgh, Pittsburgh, Pennsylvania 15260, United States*

Judith C. Yang − *Department of Chemical and Petroleum Engineering, University of Pittsburgh, Pittsburgh, Pennsylvania 15260, United States*

Graeme Henkelman − *Department of Chemistry and Oden Institute for Computational Engineering & Sciences, University of Texas at Austin, Austin, Texas 78712, United States;* orcid.org/0000-0002-0336-7153

Complete contact information is available at: https://pubs.acs.org/10.1021/acs.jctc.2c00303

Notes

The authors declare no competing financial interest.

■ ACKNOWLEDGMENTS

This work was funded from NSF (DMR-1809085, CHE-210231, and CMMI-1905647) as well as resources and collaboration from the University of Pittsburgh's Computational Resource Cluster (CRC), the Texas Advanced Computing Center, and the Theoretical Division T-1 of Los Alamos National Laboratory.

■ REFERENCES

(1) Bardi, U. The atomic structure of alloy surfaces and surface alloys. *Rep. Prog. Phys.* **1994**, *57*, 939−987.

(2) Brongersma, H. H.; Sparnaay, M. J.; Buck, T. M. Surface segregation in Cu-Ni and Cu-Pt alloys; A comparison of low-energy ion-scattering results with theory. *Surf. Sci.* **1978**, *71*, 657−678.

(3) Erdélyi, Z.; Girardeaux, C.; Tôkei, Z.; Beke, D. L.; Cserháti, C.; Rolland, A. Investigation of the interplay of nickel dissolution and copper segregation in Ni/Cu(111) system. *Surf. Sci.* **2002**, *496*, 129−140.

(4) Landa, A.; Wynblatt, P.; Girshick, A.; Vitek, V.; Ruban, A.; Skriver, H. Development of Finnis−Sinclair type potentials for Pb, Pb−Bi, and Pb−Ni systems: application to surface segregation. *Acta Mater.* **1998**, *46*, 3027−3032.

(5) Jiang, C.; Gleeson, B. Surface segregation of Pt in γ'-Ni3Al: A first-principles study. *Acta Mater.* **2007**, *55*, 1641−1647.

(6) Zhevnenko, S. N.; Petrov, I. S.; Scheiber, D.; Razumovskiy, V. I. Surface and segregation energies of Ag based alloys with Ni, Co and Fe: Direct experimental measurement and DFT study. *Acta Mater.* **2021**, *205*, No. 116565.

(7) Voter, A. F.; Montalenti, F.; Germann, T. C. Extending the Time Scale in Atomistic Simulation of Materials. *Annu. Rev. Mater. Res.* **2002**, *32*, 321−346.

(8) Miron, R. A.; Fichthorn, K. A. Multiple-Time Scale Accelerated Molecular Dynamics: Addressing the Small-Barrier Problem. *Phys. Rev. Lett.* **2004**, *93*, No. 128301.

(9) Montalenti, F.; Sørensen, M. R.; Voter, A. F. Closing the Gap between Experiment and Theory: Crystal Growth by Temperature Accelerated Dynamics. *Phys. Rev. Lett.* **2001**, *87*, No. 126101.

(10) Zamora, R. J.; Uberuaga, B. P.; Perez, D.; Voter, A. F. The Modern Temperature-Accelerated Dynamics Approach. *Annu. Rev. Chem. Biomol. Eng.* **2016**, *7*, 87−110.

(11) Perez, D.; Cubuk, E. D.; Waterland, A.; Kaxiras, E.; Voter, A. F. Long-Time Dynamics through Parallel Trajectory Splicing. *J. Chem. Theory Comput.* **2016**, *12*, 18−28.

(12) Henkelman, G.; Jónsson, H. Long time scale kinetic Monte Carlo simulations without lattice approximation and predefined event table. *J. Chem. Phys.* **2001**, *115*, 9657−9666.

(13) Lavrentiev, M. Y.; Allan, N. L.; Harding, J. H.; Harris, D. J.; Purton, J. A. Atomistic simulations of surface diffusion and segregation in ceramics. *Comput. Mater. Sci.* **2006**, *36*, 54−59.

(14) Li, L.; Li, X.; Duan, Z.; Meyer, R. J.; Carr, R.; Raman, S.; Koziol, L.; Henkelman, G. Adaptive kinetic Monte Carlo simulations of surface segregation in PdAu nanoparticles. *Nanoscale* **2019**, *11*, 10524−10535.

(15) Ida, M. P.; Miksis, M. J. The Dynamics of Thin Films I: General Theory. *SIAM J. Appl. Math.* **1998**, *58*, 456−473.

(16) Weinberger, P.; Vernes, A.; Szunyogh, L.; Zabloudil, J. Describing surfaces: Semi-infinite versus thin film approaches. *Phys. Rev. B* **2009**, *80*, No. 075430.

(17) Wang, Q.; Wang, X.; Liu, J.; Yang, Y. Cu−Ni core−shell nanoparticles: structure, stability, electronic, and magnetic properties: a spin-polarized density functional study. *J. Nanopart. Res.* **2017**, *19*, 25.

(18) Austin, N.; Butina, B.; Mpourmpakis, G. CO_2 activation on bimetallic CuNi nanoparticles. *Prog. Nat. Sci.: Mater. Int.* **2016**, *26*, 487−492.

(19) Ferasat, K.; Osetsky, Y. N.; Barashev, A. V.; Zhang, Y.; Yao, Z.; Béland, L. K. Accelerated kinetic Monte Carlo: A case study; vacancy and dumbbell interstitial diffusion traps in concentrated solid solution alloys. *J. Chem. Phys.* **2020**, *153*, No. 074109.

(20) Helander, T.; Ågren, J. A phenomenological treatment of diffusion in Al−Fe and Al−Ni alloys having B2-b.c.c. ordered structure. *Acta Mater.* **1999**, *47*, 1141−1152.

(21) Osetsky, Y. N.; Béland, L. K.; Stoller, R. E. Specific features of defect and mass transport in concentrated fcc alloys. *Acta Mater.* **2016**, *115*, 364−371.

(22) Hennes, M.; Buchwald, J.; Ross, U.; Lotnyk, A.; Mayr, S. G. Equilibrium segregation patterns and alloying in Cu/Ni nanoparticles: Experiments versus modeling. *Phys. Rev. B* **2015**, *91*, No. 245401.

(23) Webber, P. R.; Morris, M. A.; Zhang, Z. G. Crystal-face specificity in surface segregation of CuNi alloys. *J. Phys. F: Met. Phys.* **1986**, *16*, 413−419.
(24) Jin, T.; Zhang, W.; Li, N.; Liu, X.; Han, L.; Dai, W. Surface Characterization and Corrosion Behavior of 90/10 Copper-Nickel Alloy in Marine Environment. *Materials* **2019**, *12*, 1869.
(25) Tuck, C. D. S.; Powell, C. A.; Nuttall, J. Corrosion of Copper and Its Alloys. In *Reference Module in Materials Science and Materials Engineering*; Elsevier, 2016.
(26) Zegkinoglou, I.; Pielsticker, L.; Han, Z.; Divins, N. J.; Kordus, D.; Chen, Y.; Escudero, C.; Pérez-Dieste, V.; Zhu, B.; Gao, Y.; Cuenya, B. R. Surface Segregation in CuNi Nanoparticle Catalysts During CO2 Hydrogenation: The Role of CO in the Reactant Mixture. *J. Phys. Chem. C* **2019**, *123*, 8421−8428.
(27) Tan, Q.; Shi, Z.; Wu, D. CO_2 Hydrogenation to Methanol over a Highly Active Cu−Ni/CeO_2−Nanotube Catalyst. *Ind. Eng. Chem. Res.* **2018**, *57*, 10148−10158.
(28) Lortie, M.; Isaifan, R.; Liu, Y.; Mommers, S. Synthesis of CuNi/C and CuNi/-Al_2O_3 Catalysts for the Reverse Water Gas Shift Reaction. *Int. J. Chem. Eng.* **2015**, No. 750689.
(29) Good, B.; Bozzolo, G.; Ferrante, J. Surface segregation in Cu-Ni alloys. *Phys. Rev. B* **1993**, *48*, 18284−18287.
(30) Foiles, S. M. Calculation of the surface segregation of Ni-Cu alloys with the use of the embedded-atom method. *Phys. Rev. B* **1985**, *32*, 7685−7693.
(31) Tréglia, G.; Legrand, B.; Maugain, P. Surface segregation in CuNi and AgNi alloys formulated as an area-preserving map. *Surf. Sci.* **1990**, *225*, 319−330.
(32) Panizon, E.; Olmos-Asar, A. J.; Peressi, M.; Ferrando, R. Study of structures and thermodynamics of CuNi nanoalloys using a new DFT-fitted atomistic potential. *Phys. Chem. Chem. Phys.* **2015**, *17*, 28068−28075.
(33) Xiang, M.; Liao, Y.; Wang, K.; Lu, G.; Chen, J. Shock-induced plasticity in semi-coherent {111} Cu-Ni multilayers. *Int. J. Plast.* 2018, *103*, 23−38. DOI: 10.1016/j.ijplas.2017.12.005.
(34) Perez, D.; Uberuaga, B. P.; Voter, A. F. The parallel replica dynamics method - Coming of age. *Comput. Mater. Sci.* **2015**, *100*, 90−103.
(35) Voter, A. F. Parallel replica method for dynamics of infrequent events. *Phys. Rev. B* **1998**, *57*, 13985−13988.
(36) Perez, D.; Huang, R.; Voter, A. F. Long-time molecular dynamics simulations on massively parallel platforms: A comparison of parallel replica dynamics and parallel trajectory splicing. *J. Mater. Res.* **2018**, *33*, 813−822.
(37) Le Bris, C.; Lelievre, T.; Luskin, M.; Perez, D. A mathematical formalization of the parallel replica dynamics. *Monte Carlo Methods and Applications* **2012**, *18*, 119−146.
(38) Xu, L.; Henkelman, G. Adaptive kinetic Monte Carlo for first-principles accelerated dynamics. *J. Chem. Phys.* **2008**, *129*, 114104.
(39) Henkelman, G.; Jónsson, H. A dimer method for finding saddle points on high dimensional potential surfaces using only first derivatives. *J. Chem. Phys.* **1999**, *111*, 7010−7022.
(40) Kästner, J.; Sherwood, P. Superlinearly converging dimer method for transition state search. *J. Chem. Phys.* **2008**, *128*, No. 014106.
(41) Heyden, A.; Bell, A. T.; Keil, F. J. Efficient methods for finding transition states in chemical reactions: Comparison of improved dimer method and partitioned rational function optimization method. *J. Chem. Phys.* **2005**, *123*, 224101.
(42) Fischer, F.; Schmitz, G.; Eich, S. M. A systematic study of grain boundary segregation and grain boundary formation energy using a new copper−nickel embedded-atom potential. *Acta Mater.* **2019**, *176*, 220−231.
(43) Kresse, G.; Furthmüller, J. Efficient iterative schemes for ab initio total-energy calculations using a plane-wave basis set. *Phys. Rev. B* **1996**, *54*, 11169−11186.
(44) Kresse, G.; Furthmüller, J. Efficiency of ab-initio total energy calculations for metals and semiconductors using a plane-wave basis set. *Comput. Mater. Sci.* **1996**, *6*, 15−50.
(45) Kresse, G.; Joubert, D. From ultrasoft pseudopotentials to the projector augmented-wave method. *Phys. Rev. B* **1999**, *59*, 1758−1775.
(46) Perdew, J. P.; Burke, K.; Ernzerhof, M. Generalized Gradient Approximation Made Simple. *Phys. Rev. Lett.* **1996**, *77*, 3865−3868.
(47) Blöchl, P. E. Projector augmented-wave method. *Phys. Rev. B* **1994**, *50*, 17953−17979.
(48) Ruban, A. V.; Skriver, H. L.; Nørskov, J. K. Surface segregation energies in transition-metal alloys. *Phys. Rev. B* **1999**, *59*, 15990−16000.
(49) Beichl, I.; Sullivan, F. The Metropolis Algorithm. *Comput. Sci. Eng.* **2000**, *2*, 65−69.
(50) Sakurai, T.; Hashizume, T.; Jimbo, A.; Sakai, A.; Hyodo, S. New result in surface segregation of Ni-Cu binary alloys. *Phys. Rev. Lett.* **1985**, *55*, 514−517.
(51) Plimpton, S. Fast Parallel Algorithms for Short-Range Molecular Dynamics. *J. Comput. Phys.* **1995**, *117*, 1−19.
(52) Sheppard, D.; Terrell, R.; Henkelman, G. Optimization methods for finding minimum energy paths. *J. Chem. Phys.* **2008**, *128*, 134106.
(53) Henkelman, G.; Jónsson, H. *EON: Long timescale dynamics*, 2021; https://theory.cm.utexas.edu/eon/.
(54) Lam, N. Q.; Dagens, L.; Doan, N. V. Calculations of the properties of self-interstitials and vacancies in the face-centred cubic metals Cu, Ag and Au. *J. Phys. F: Met. Phys.* **1983**, *13*, 2503−2516.
(55) Novotny, M. A. Monte Carlo Algorithms with Absorbing Markov Chains: Fast Local Algorithms for Slow Dynamics. *Phys. Rev. Lett.* **1995**, *74*, 1−5.
(56) Zhang, L.; Han, J.; Wang, H.; Saidi, W. A.; Car, R.; Weinan, E. *End-to-end symmetry preserving inter-atomic potential energy model for finite and extended systems*. In Proceedings of the 32nd International Conference on Neural Information Processing Systems, Montréal, Canada; 2018.
(57) Andolina, C. M.; Williamson, P.; Saidi, W. A. Optimization and validation of a deep learning CuZr atomistic potential: Robust applications for crystalline and amorphous phases with near-DFT accuracy. *J. Chem. Phys.* **2020**, *152*, 154701.
(58) Andolina, C. M.; Bon, M.; Passerone, D.; Saidi, W. A. Robust, Multi-Length-Scale, Machine Learning Potential for Ag−Au Bimetallic Alloys from Clusters to Bulk Materials. *J. Phys. Chem. C* **2021**, *125*, 17438−17447.
(59) Andolina, C. M.; Wright, J. G.; Das, N.; Saidi, W. A. Improved Al-Mg alloy surface segregation predictions with a machine learning atomistic potential. *Phys. Rev. Mater.* **2021**, *5*, No. 083804.
(60) Bayerl, D.; Andolina, C. M.; Dwaraknath, S.; Saidi, W. A. Convergence acceleration in machine learning potentials for atomistic simulations. *Digital Discovery* **2022**, *1*, 61−69.